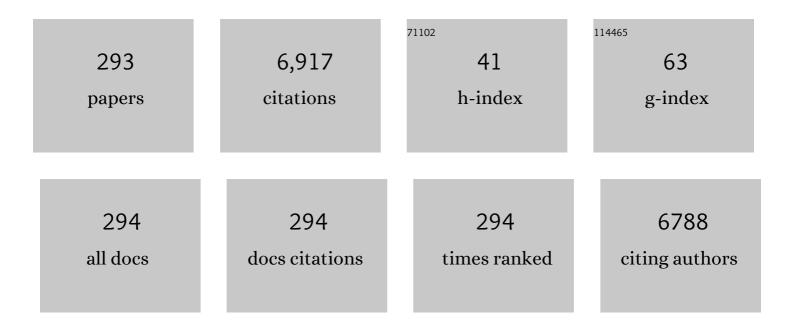
## Sea-Fue Wang

List of Publications by Year in descending order

Source: https://exaly.com/author-pdf/1876178/publications.pdf Version: 2024-02-01



#	Article	IF	CITATIONS
1	Unipolar resistive switching characteristics of ZnO thin films for nonvolatile memory applications. Applied Physics Letters, 2008, 92, .	3.3	417
2	Fabrication of hierarchical NiCo2S4@CoS2 nanostructures on highly conductive flexible carbon cloth substrate as a hybrid electrode material for supercapacitors with enhanced electrochemical performance. Electrochimica Acta, 2019, 293, 328-337.	5.2	169
3	Effect of Various Deep Eutectic Solvents on the Sustainable Synthesis of MgFe <sub>2</sub> O <sub>4</sub> Nanoparticles for Simultaneous Electrochemical Determination of Nitrofurantoin and 4-Nitrophenol. ACS Sustainable Chemistry and Engineering, 2020, 8, 1479-1486.	6.7	124
4	Densification and microwave dielectric properties of CaO–B2O3–SiO2 system glass–ceramics. Ceramics International, 2008, 34, 599-604.	4.8	115
5	Dielectric Properties of Fineâ€Grained Barium Titanate Based X7R Materials. Journal of the American Ceramic Society, 1999, 82, 2677-2682.	3.8	114
6	Electrodeposition of copper nanoparticles using pectin scaffold at graphene nanosheets for electrochemical sensing of glucose and hydrogen peroxide. Electrochimica Acta, 2015, 176, 804-810.	5.2	101
7	Facile sonochemical synthesis of perovskite-type SrTiO3 nanocubes with reduced graphene oxide nanocatalyst for an enhanced electrochemical detection of α-amino acid (tryptophan). Ultrasonics Sonochemistry, 2019, 56, 193-199.	8.2	96
8	ZnO nanowire-based CO sensors prepared on patterned ZnO:Ga/SiO2/Si templates. Sensors and Actuators B: Chemical, 2007, 125, 498-503.	7.8	85
9	Preparation and characterization of copper nanoparticles/zinc oxide composite modified electrode and its application to glucose sensing. Materials Science and Engineering C, 2010, 30, 86-91.	7.3	84
10	Eutectic Solvent-Mediated Synthesis of NiFe-LDH/Sulfur-Doped Carbon Nitride Arrays: Investigation of Electrocatalytic Activity for the Dimetridazole Sensor in Human Sustenance. ACS Sustainable Chemistry and Engineering, 2020, 8, 17772-17782.	6.7	84
11	Synthesis of magnetic Fe 3 O 4 /activated carbon nanocomposites with high surface area as recoverable adsorbents. Journal of the Taiwan Institute of Chemical Engineers, 2018, 90, 51-60.	5.3	81
12	Integration of samarium vanadate/carbon nanofiber through synergy: An electrochemical tool for sulfadiazine analysis. Journal of Hazardous Materials, 2021, 408, 124940.	12.4	80
13	Effect of Ag on the microstructure and electrical properties of ZnO. Journal of the European Ceramic Society, 2007, 27, 4521-4527.	5.7	77
14	Determination of acoustic wave velocities and elastic properties for diamond and other hard materials. Materials Chemistry and Physics, 2004, 85, 432-437.	4.0	76
15	Morphology-controllable Bi2O3 crystals through an aqueous precipitation method and their photocatalytic performance. Dyes and Pigments, 2013, 98, 25-30.	3.7	76
16	Densification and properties of fluxed sintered NiCuZn ferrites. Journal of Magnetism and Magnetic Materials, 2000, 217, 35-43.	2.3	72
17	Reduction behaviors and catalytic properties for methanol steam reforming of Cu-based spinel compounds CuX2O4 (X=Fe, Mn, Al, La). Ceramics International, 2014, 40, 4541-4551.	4.8	72
18	Thermal properties and flammability of polylactide nanocomposites with aluminum trihydrate and organoclay. Carbohydrate Polymers, 2012, 87, 1119-1123.	10.2	69

#	Article	IF	CITATIONS
19	Characterizations of CaO–B2O3–SiO2 glass–ceramics: Thermal and electrical properties. Journal of Alloys and Compounds, 2008, 461, 612-616.	5.5	68
20	Facile synthesis of copper sulfide decorated reduced graphene oxide nanocomposite for high sensitive detection of toxic antibiotic in milk. Ultrasonics Sonochemistry, 2019, 52, 382-390.	8.2	65
21	A screen-printed electrode modified with tungsten disulfide nanosheets for nanomolar detection of the arsenic drug roxarsone. Mikrochimica Acta, 2019, 186, 420.	5.0	62
22	Densification and magnetic properties of low-fire NiCuZn ferrites. Journal of Magnetism and Magnetic Materials, 2000, 220, 129-138.	2.3	60
23	Characterization of samarium-doped ceria powders prepared by hydrothermal synthesis for use in solid state oxide fuel cells. Journal of Materials Research and Technology, 2013, 2, 141-148.	5.8	58
24	Engineering Architecture of 3D-Urchin-like Structure and 2D-Nanosheets of Bi <sub>2</sub> S <sub>3</sub> @g-C <sub>3</sub> N <sub>4</sub> as the Electrode Material for a Solid-State Symmetric Supercapacitor. Energy & Fuels, 2021, 35, 12569-12580.	5.1	56
25	Interfacial Superassembly of Mo <sub>2</sub> C@NiMn-LDH Frameworks for Electrochemical Monitoring of Carbendazim Fungicide. ACS Sustainable Chemistry and Engineering, 2021, 9, 14900-14910.	6.7	56
26	Effects of additives on the loss characteristics of Mn–Zn ferrite. Journal of Magnetism and Magnetic Materials, 2014, 365, 119-125.	2.3	53
27	A novel electrochemical sensor for determination of DNA damage biomarker (8-hydroxy-2′-deoxyguanosine) in urine using sonochemically derived graphene oxide sheets covered zinc oxide flower modified electrode. Ultrasonics Sonochemistry, 2019, 58, 104622.	8.2	53
0.0	Surface Engineering of Three-Dimensional-like Hybrid AB <sub>2</sub> O <sub>4</sub> (AB = Zn, Co, and) Tj ET		
28	Electrocatalyst for Clioquinol Detection. ACS Applied Electronic Materials, 2021, 3, 362-372.	4.3	53
29	Characteristics of polyimide/barium titanate composite films. Ceramics International, 2009, 35, 265-268.	4.8	52
30	Ultrasound-assisted synthesis of tungsten trioxide entrapped with graphene nanosheets for developing nanomolar electrochemical (hormone) sensor and enhanced sensitivity of the catalytic performance. Ultrasonics Sonochemistry, 2019, 56, 134-142.	8.2	51
31	Effect of ZnO seed layers on the solution chemical growth of ZnO nanorod arrays. Ceramics International, 2009, 35, 1255-1260.	4.8	50
32	Effect of additives on the thermal properties and sealing characteristic of BaO-Al2O3-B2O3-SiO2 glass-ceramic for solid oxide fuel cell application. International Journal of Hydrogen Energy, 2009, 34, 8235-8244.	7.1	50
33	Structural Characterization and Luminescent Properties of a Red Phosphor Series: Y <sub>2a^'<i>x</i></sub> Eu <sub>x</sub> (MoO <sub>4</sub> ) <sub>3</sub> (x=0.4–2.0). Journal of the American Ceramic Society, 2009, 92, 1732-1738.	3.8	49
34	Acid yellow 9 as a dispersing agent for carbon nanotubes: Preparation of redox polymer–carbon nanotube composite film and its sensing application towards ascorbic acid and dopamine. Biosensors and Bioelectronics, 2010, 25, 2592-2597.	10.1	49
35	Deep eutectic solvent-based manganese molybdate nanosheets for sensitive and simultaneous detection of human lethal compounds: comparing the electrochemical performances of M-molybdate (M = Mg, Fe, and Mn) electrocatalysts. Nanoscale, 2020, 12, 19719-19731.	5.6	49
36	Mechanical Properties of Microcellular and Nanocellular Thermoplastic Polyurethane Nanocomposite Foams Created Using Supercritical Carbon Dioxide. Industrial & Engineering Chemistry Research, 2017, 56, 8499-8507.	3.7	48

#	Article	IF	CITATIONS
37	Novel sonochemical synthesis of Fe3O4 nanospheres decorated on highly active reduced graphene oxide nanosheets for sensitive detection of uric acid in biological samples. Ultrasonics Sonochemistry, 2019, 58, 104618.	8.2	48
38	Effect of glass composition on the densification and dielectric properties of BaTiO3 ceramics. Ceramics International, 2001, 27, 157-162.	4.8	47
39	Synergy of the LaVO <sub>4</sub> /h-BN Nanocomposite: A Highly Active Electrocatalyst for the Rapid Analysis of Carbendazim. Inorganic Chemistry, 2021, 60, 5271-5281.	4.0	47
40	Couroupita guianansis dead flower derived porous activated carbon as efficient supercapacitor electrode material. Materials Research Bulletin, 2019, 112, 390-398.	5.2	46
41	Thermoplastic polyurethane/clay nanocomposite foam made by batch foaming. Journal of Cellular Plastics, 2013, 49, 119-130.	2.4	44
42	MnCo <sub>2</sub> O <sub>4</sub> Microflowers Anchored on P-Doped <i>g</i> -C <sub>3</sub> N <sub>4</sub> Nanosheets as an Electrocatalyst for Voltammetric Determination of the Antibiotic Drug Sulfadiazine. ACS Applied Electronic Materials, 2021, 3, 3915-3926.	4.3	44
43	Effects of Zr addition on the microstructure and mechanical behavior of a fine-grained nickel-based superalloy at elevated temperatures. Materials Science & Engineering A: Structural Materials: Properties, Microstructure and Processing, 2014, 607, 294-301.	5.6	43
44	Dielectric properties and microstructures of non-reducible high-temperature stable X9R ceramics. Journal of the European Ceramic Society, 2013, 33, 1793-1799.	5.7	42
45	Effects of Preparation Conditions on the Growth of ZnO Nanorod Arrays Using Aqueous Solution Method. International Journal of Applied Ceramic Technology, 2008, 5, 419-429.	2.1	41
46	Deposition of low-resistivity gallium-doped zinc oxide films by low-temperature radio-frequency magnetron sputtering. Thin Solid Films, 2009, 517, 6310-6314.	1.8	40
47	Characterization of boron-doped diamond-like carbon prepared by radio frequency sputtering. Thin Solid Films, 2010, 519, 521-526.	1.8	40
48	Fabrication of electrolyte supported micro-tubular SOFCs using extrusion and dip-coating. International Journal of Hydrogen Energy, 2013, 38, 2859-2867.	7.1	40
49	Cobalt molybdate nanorods decorated on boron-doped graphitic carbon nitride sheets for electrochemical sensing of furazolidone. Mikrochimica Acta, 2020, 187, 654.	5.0	40
50	Liquid-phase sintering and chemical inhomogeneity in the BaTiO3–BaCO3–LiF system. Journal of Materials Research, 2000, 15, 407-416.	2.6	38
51	Highly selective and sensitive fluorescent chemosensor for femtomolar detection of silver ion in aqueous medium. Sensing and Bio-Sensing Research, 2015, 6, 19-24.	4.2	37
52	Well-Designed Construction of Yttrium Orthovanadate Confined on Graphitic Carbon Nitride Sheets: Electrochemical Investigation of Dimetridazole. Inorganic Chemistry, 2021, 60, 13150-13160.	4.0	37
53	Versatile deep eutectic solvent assisted synthesis of ZnB2O4 (BÂ=ÂAl, Co, Cr) spinels: The effect of B site variants for comparing the bifunctional electrochemical sensing application. Chemical Engineering Journal, 2022, 435, 134136.	12.7	37
54	High-temperature oxidation behaviors of CVD diamond films. Applied Surface Science, 2009, 256, 668-673.	6.1	36

#	Article	IF	CITATIONS
55	Catalysts prepared from copper–nickel ferrites for the steam reforming of methanol. Journal of Power Sources, 2015, 281, 138-145.	7.8	36
56	Femtomolar detection of mercuric ions using polypyrrole, pectin and graphene nanocomposites modified electrode. Journal of Colloid and Interface Science, 2016, 483, 268-274.	9.4	35
57	Hexagonal Ba(Ti1â^'xMnx)O3 ceramics: Microstructural evolution and microwave dielectric properties. Applied Physics Letters, 2006, 88, 042909.	3.3	34
58	Effects of Metallo-Organic Decomposition Agents on Thermal Decomposition and Electrical Conductivity of Low-Temperature-Curing Silver Paste. Japanese Journal of Applied Physics, 2006, 45, 6987-6992.	1.5	33
59	Densification and microwave dielectric behaviors of CaO–B2O3–SiO2 glass-ceramics prepared from a binary glass composite. Journal of Alloys and Compounds, 2010, 498, 211-216.	5.5	33
60	Characteristics of Cu and Mo-doped Ca3Co4O9â^ cathode materials for use in solid oxide fuel cells. Ceramics International, 2016, 42, 11239-11247.	4.8	33
61	Lanthanide type of cerium sulfide embedded carbon nitride composite modified electrode for potential electrochemical detection of sulfaguanidine. Mikrochimica Acta, 2021, 188, 313.	5.0	33
62	Electrosynthesis and characterization of lead oxide thin films. Materials Characterization, 2007, 58, 817-822.	4.4	32
63	Effects of sonochemical approach and induced contraction of core–shell bismuth sulfide/graphitic carbon nitride as an efficient electrode materials for electrocatalytic detection of antibiotic drug in foodstuffs. Ultrasonics Sonochemistry, 2021, 72, 105445.	8.2	32
64	Facile solid-state synthesis of layered molybdenum boride-based electrode for efficient electrochemical aqueous asymmetric supercapacitor. Journal of Alloys and Compounds, 2021, 877, 160192.	5.5	32
65	One-Pot Green Recovery of Copper Oxide nanoparticles from Discarded Printed Circuit Boards for electrode material in Supercapacitor Application. Resources, Conservation and Recycling, 2022, 180, 106180.	10.8	32
66	Characterization of the Low-Curing-Temperature Silver Paste with Silver 2-Ethylhexanoate Addition. Japanese Journal of Applied Physics, 2007, 46, 251-255.	1.5	31
67	Properties of Hexagonal Ba(Ti1-xMnx)O3Ceramics: Effects of Sintering Temperature and Mn Content. Japanese Journal of Applied Physics, 2007, 46, 2978-2983.	1.5	31
68	Poly(BCB)/Au-nanoparticles hybrid film modified electrode: Preparation, characterization and its application as a non-enzymatic sensor. Thin Solid Films, 2010, 518, 5832-5838.	1.8	31
69	Investigation of nitrogen doped diamond like carbon films as counter electrodes in dye sensitized solar cells. Journal of Alloys and Compounds, 2011, 509, 1969-1974.	5.5	31
70	Sea-Urchin-Like Bi <sub>2</sub> S <sub>3</sub> Microstructures Decorated with Graphitic Carbon Nitride Nanosheets for Use in Food Preservation. ACS Applied Nano Materials, 2022, 5, 2375-2384.	5.0	31
71	ZnO Nanowire-Based CO Sensors Prepared at Various Temperatures. Journal of the Electrochemical Society, 2007, 154, J393.	2.9	30
72	The phase stability and electrical conductivity of Bi2O3 ceramics stabilized by Co-dopants. Journal of Power Sources, 2012, 218, 106-112.	7.8	30

#	Article	IF	CITATIONS
73	Effects of bi-layer La0.6Sr0.4Co0.2Fe0.8O3â^´Î´-based cathodes on characteristics of intermediate temperature solid oxide fuel cells. Journal of Power Sources, 2011, 196, 977-987.	7.8	29
74	Electrochemical determination of caffeic acid in antioxidant beverages samples via a facile synthesis of carbon/iron-based active electrocatalyst. Analytica Chimica Acta, 2020, 1122, 76-88.	5.4	29
75	Electrochemical sensor-based barium zirconate on sulphur-doped graphitic carbon nitride for the simultaneous determination of nitrofurantoin (antibacterial agent) and nilutamide (anticancer drug). Journal of Electroanalytical Chemistry, 2021, 901, 115782.	3.8	29
76	Effects of Silver Oxide Addition on the Electrical Resistivity and Microstructure of Low-Temperature-Curing Metallo-Organic Decomposition Silver Pastes. Japanese Journal of Applied Physics, 2007, 46, 4179-4183.	1.5	28
77	Flammability and tensile properties of polylactide nanocomposites with short carbon fibers. Journal of Materials Science, 2015, 50, 1605-1612.	3.7	27
78	Simple electrochemical growth of copper nanoparticles decorated silver nanoleaves for the sensitive determination of hydrogen peroxide in clinical lens cleaning solutions. Sensors and Actuators B: Chemical, 2017, 252, 862-869.	7.8	27
79	Direct pyrolysis and ultrasound assisted preparation of N, S co-doped graphene/Fe3C nanocomposite as an efficient electrocatalyst for oxygen reduction and oxygen evolution reactions. Ultrasonics Sonochemistry, 2020, 66, 105111.	8.2	27
80	Toward the Development of Disposable Electrodes Based on Holmium Orthovanadate/ <i>f</i> -Boron Nitride: Impacts and Electrochemical Performances of Emerging Inorganic Contaminants. Inorganic Chemistry, 2021, 60, 12425-12435.	4.0	27
81	Surfactant-Assisted Synthesis of Praseodymium Orthovanadate Nanofiber-Supported NiFe-Layered Double Hydroxide Bifunctional Catalyst: The Electrochemical Detection and Degradation of Diphenylamine. Inorganic Chemistry, 2022, 61, 5824-5835.	4.0	27
82	Characteristics of SrCo1â^'xSnxO3â^'δ cathode materials for use in solid oxide fuel cells. Solid State Ionics, 2012, 227, 10-16.	2.7	26
83	Effect of dispersion method and process variables on the properties of supercritical CO <sub>2</sub> foamed polystyrene/graphite nanocomposite foam. Polymer Engineering and Science, 2013, 53, 2061-2072.	3.1	26
84	Effects of co-dopants on the magnetic properties of Ni–Zn ferrites. Journal of Magnetism and Magnetic Materials, 2015, 374, 402-410.	2.3	26
85	Facile Synthesis of Tungsten Carbide Nanosheets for Trace Level Detection of Toxic Mercury Ions in Biological and Contaminated Sewage Water Samples: An Electrocatalytic Approach. Journal of the Electrochemical Society, 2019, 166, B761-B770.	2.9	26
86	Hydrothermally synthesized cubical zinc manganite nanostructure for electrocatalytic detection of sulfadiazine. Mikrochimica Acta, 2021, 188, 131.	5.0	26
87	Sustainable synthesis of AFe <sub>2</sub> O <sub>4</sub> (A = Mg, Zn, Mn) catalysts: comparing the photooxidative and electrochemical properties towards organic dyes detection and degradation. New Journal of Chemistry, 2021, 45, 10049-10056.	2.8	26
88	Effects of SnO2, WO3, and ZrO2 addition on the magnetic and mechanical properties of NiCuZn ferrites. Journal of Magnetism and Magnetic Materials, 2015, 374, 381-387.	2.3	25
89	A ternary nanocomposite based on nickel( <scp>iii</scp> ) oxide@f-CNF/rGO for efficient electrochemical detection of an antipsychotic drug (Klonopin) in biological samples. New Journal of Chemistry, 2020, 44, 10250-10257.	2.8	25
90	Layered nanocomposite of zinc sulfide covered reduced graphene oxide and their implications for electrocatalytic applications. Ultrasonics Sonochemistry, 2020, 64, 105036.	8.2	25

#	Article	IF	CITATIONS
91	Novel voltammetric detection of norfloxacin in urine and blood serum using a flexible Ni foam based Ni-Co-MOF ultrathin nanosheets derived from Ni-Co-LDH. Microchemical Journal, 2021, 160, 105747.	4.5	25
92	Fabrication of Co <sub>3</sub> O <sub>4</sub> nanoparticle-decorated porous activated carbon electrode for the electrochemical detection of 4-nitrophenol. New Journal of Chemistry, 2021, 45, 18358-18365.	2.8	25
93	Electrochemical detection of antipsychotic drug in water samples based on nano/sub-microrod-like CuBi2â^'xInxO4 electrocatalysts. Microchemical Journal, 2021, 163, 105886.	4.5	25
94	Densification, microstructural evolution, and dielectric properties of hexagonal Ba(Ti1â^'xMnx)O3 ceramics sintered with fluxes. Journal of Alloys and Compounds, 2009, 480, 499-504.	5.5	24
95	A New Route for the Enzymeless Trace Level Detection of Creatinine Based on Reduced Graphene Oxide/Silver Nanocomposite Biosensor. Electroanalysis, 2017, 29, 559-565.	2.9	24
96	Rationally designed RGO@CuO@Mn <sub>2</sub> O <sub>3</sub> as an excellent electrocatalyst for the rapid and real-time detection of 2-nitrophenol. New Journal of Chemistry, 2020, 44, 12465-12472.	2.8	24
97	Revealing the effect of multidimensional ZnO@CNTs/RGO composite for enhanced electrochemical detection of flufenamic acid. Microchemical Journal, 2021, 168, 106448.	4.5	24
98	The simultaneous electrochemical determination of furazolidone and dimetridazole using transition metal titanates with an ilmenite type structure. Journal of Materials Chemistry C, 2021, 9, 15263-15275.	5.5	24
99	Synchronously activated strontium aluminate nanoflakes anchored functionalized carbon nanofiber nanocomposite for sensitive amperometric detection of food additive: Propyl gallate. Food Chemistry, 2022, 389, 133119.	8.2	24
100	La2O3–Al2O3–B2O3–SiO2 glasses for solid oxide fuel cell applications. International Journal of Hydrogen Energy, 2011, 36, 3666-3672.	7.1	23
101	B2O3-free SiO2–Al2O3–SrO–La2O3–ZnO–TiO2 glass sealants for intermediate temperature solid oxid fuel cell applications. International Journal of Hydrogen Energy, 2012, 37, 5901-5913.	de <sub>7.1</sub>	23
102	Densification, microstructure evolution, and microwave dielectric properties of Mg 1-x Ca x ZrTa 2 O 8 ceramics. Journal of the European Ceramic Society, 2017, 37, 2825-2831.	5.7	23
103	Direct electron transfer of cytochrome C and its electrocatalytic properties on multiwalled carbon nanotubes/ciprofloxacin films. Journal of Solid State Electrochemistry, 2010, 14, 2129-2135.	2.5	22
104	Characteristics of electrolyte supported micro-tubular solid oxide fuel cells with GDC-ScSZ bilayer electrolyte. International Journal of Hydrogen Energy, 2014, 39, 17267-17274.	7.1	22
105	Preparation of Co-MOF derived Co(OH)2/multiwalled carbon nanotubes as an efficient bifunctional electro catalyst for hydrazine and hydrogen peroxide detections. Journal of the Taiwan Institute of Chemical Engineers, 2018, 93, 79-86.	5.3	22
106	A simple chemical approach for synthesis of Sr2Co2O5 nanoparticles and its application in the detection of chloramphenicol and in energy storage systems. Journal of Electroanalytical Chemistry, 2021, 880, 114911.	3.8	22
107	Surface engineering of roselike lanthanum molybdate electrocatalyst modified screen-printed carbon electrode for robust and highly sensitive sensing of antibiotic drug. Microchemical Journal, 2021, 164, 106044.	4.5	22
108	Zirconium Phosphate Supported on g-C <sub>3</sub> N <sub>4</sub> Nanocomposite for Sensitive Detection of Nitrite. Journal of the Electrochemical Society, 2021, 168, 087502.	2.9	22

#	Article	IF	CITATIONS
109	Characterization of chromium thin films by sputter deposition. Journal of Alloys and Compounds, 2011, 509, 10110-10114.	5.5	21
110	Highly sensitive determination of cancer toxic mercury ions in biological and human sustenance samples based on green and robust synthesized stannic oxide nanoparticles decorated reduced graphene oxide sheets. Analytica Chimica Acta, 2020, 1137, 181-190.	5.4	21
111	Synthesis of core-shell-like structure SnS2-SnO2 integrated with graphene nanosheets for the electrochemical detection of furazolidone drug in furoxone tablet. Journal of Molecular Liquids, 2020, 313, 113554.	4.9	21
112	Synergistic effect of Co3O4 nanoparticles with Bauhinia vahlii dry fruits derived activated carbon on energy storage applications. Journal of Solid State Chemistry, 2021, 295, 121931.	2.9	21
113	An enhanced electrochemical performance of in milk, pigeon meat and eggs samples using se nanorods capped with Co3O4 nanoflowers decorated on graphene oxide. Colloids and Surfaces B: Biointerfaces, 2021, 200, 111577.	5.0	21
114	Synthesis of hierarchical mesoporous graphite oxide/Al 2 O 3 from MIL-100(Al) for the electrochemical determination of caffeic acid in red wine samples. Journal of the Taiwan Institute of Chemical Engineers, 2018, 84, 188-195.	5.3	20
115	Investigation of sonochemically synthesized sphere-like metal tungstate nanocrystals decorated activated carbon sheets network and its application towards highly sensitive detection of arsenic drug in biological samples. Journal of the Taiwan Institute of Chemical Engineers, 2020, 114, 211-219.	5.3	20
116	Graphene oxide@Ce-doped TiO2 nanoparticles as electrocatalyst materials for voltammetric detection of hazardous methyl parathion. Mikrochimica Acta, 2021, 188, 216.	5.0	20
117	Modification of glassy carbon electrode with manganese cobalt oxide-cubic like structures incorporated graphitic carbon nitride sheets for the voltammetric determination of 2,4,6 -trichlorophenol. Mikrochimica Acta, 2022, 189, 205.	5.0	20
118	Effective conversion of Cassia fistula dry fruits biomass into porous activated carbon for supercapacitors. Materials Chemistry and Physics, 2022, 286, 126188.	4.0	20
119	Effect of niobium doping on the densification and grain growth in alumina. Ceramics International, 2008, 34, 1183-1187.	4.8	19
120	Microstructural Investigation of Ba(Ti <sub>(1â^'x)</sub> Mn <sub>x</sub> )O <sub>3</sub> Ceramics with 6H―and 12Râ€Polytypes. Journal of the American Ceramic Society, 2009, 92, 2099-2108.	3.8	19
121	Effects of (LaSr)(CoFeCu)O3â^î^ cathodes on the characteristics of intermediate temperature solid oxide fuel cells. Journal of Power Sources, 2012, 201, 18-25.	7.8	19
122	SiO2–Al2O3–Y2O3–ZnO glass sealants for intermediate temperature solid oxide fuel cell applications. International Journal of Hydrogen Energy, 2013, 38, 14779-14790.	7.1	19
123	Electrochemical Activation of Graphite Nanosheets Decorated with Palladium Nanoparticles for High Performance Amperometric Hydrazine Sensor. Electroanalysis, 2016, 28, 808-816.	2.9	19
124	Characteristics of glass sealants for intermediate-temperature solid oxide fuel cell applications. Ceramics International, 2017, 43, S613-S620.	4.8	19
125	Copper Nanoparticle and Nitrogen Doped Graphite Oxide Based Biosensor for the Sensitive Determination of Glucose. Nanomaterials, 2018, 8, 429.	4.1	19
126	Effects of additives on the microstructure and dielectric properties of Ba <sub>2</sub> Ti <sub>9</sub> O <sub>20</sub> microwave ceramic. Journal of Materials Research, 2003, 18, 1179-1187.	2.6	18

#	Article	IF	CITATIONS
127	High-temperature oxidation behavior of nanocrystalline diamond films. Journal of Alloys and Compounds, 2010, 489, 638-644.	5.5	18
128	Effects of alloy elements on microstructure and creep properties of fine-grained nickel-based superalloys at moderate temperatures. Materials Science & Engineering A: Structural Materials: Properties, Microstructure and Processing, 2013, 571, 155-160.	5.6	18
129	Electrochemical Synthesis of β yclodextrin Functionalized Silver Nanoparticles and Reduced Graphene Oxide Composite for the Determination of Hydrazine. Electroanalysis, 2016, 28, 1970-1976.	2.9	18
130	Electrochemical preparation of biomolecule stabilized copper nanoparticles decorated reduced graphene oxide for the sensitive and selective determination of hydrogen peroxide. Electrochimica Acta, 2016, 191, 55-61.	5.2	18
131	Fabrication of highly sensitive anticancer drug sensor based on heterostructured ZnO-Co3O4 capped on carbon nitride nanomaterials. Microchemical Journal, 2021, 167, 106244.	4.5	18
132	Solvothermal synthesis of silver tungstate integrated with carbon nitrides matrix composites for highly sensitive electrochemical nitrofuran derivative sensing in biological samples. Analytica Chimica Acta, 2022, 1192, 339355.	5.4	18
133	Colloidal synthesis of perovskite-type lanthanum aluminate incorporated graphene oxide composites: Electrochemical detection of nitrite in meat extract and drinking water. Mikrochimica Acta, 2022, 189, 210.	5.0	18
134	Characterization of Inductor with Ni–Zn–Cu Ferrite Embedded in B2O3–SiO2Glass. Japanese Journal of Applied Physics, 2007, 46, 5792-5796.	1.5	17
135	Porous calcium sulfate ceramics with tunable degradation rate. Journal of Materials Science: Materials in Medicine, 2012, 23, 2437-2443.	3.6	17
136	Transition metal-doped lanthanum germanate apatites as electrolyte materials of solid oxide fuel cells. Solid State Ionics, 2013, 247-248, 48-55.	2.7	17
137	Fabrication of Strontium Molybdate Incorporated with Graphitic Carbon Nitride Composite: High-sensitive Amperometric Sensing Platform of Food Additive in Foodstuffs. Microchemical Journal, 2021, 167, 106307.	4.5	17
138	Dielectric properties of CaO–B2O3–SiO2 glass-ceramic systems in the millimeter-wave frequency range of 20–60ÂCHz. Ceramics International, 2021, 47, 22627-22635.	4.8	17
139	An electrochemical sensing of phenolic derivative 4-Cyanophenol in environmental water using a facile-constructed Aurivillius-structured Bi2MoO6. Ecotoxicology and Environmental Safety, 2021, 208, 111701.	6.0	17
140	Adsorption of ciprofloxacin and its role for stabilizing multi-walled carbon nanotubes and characterization. Materials Letters, 2009, 63, 1830-1833.	2.6	16
141	Physical and electrical properties of polyimide/ceramic hybrid films prepared via non-hydrolytic sol–gel process. Journal of Materials Science: Materials in Electronics, 2010, 21, 104-110.	2.2	16
142	Ultra‣owâ€Fire Zn <sub>2</sub> Te <sub>3</sub> O <sub>8</sub> –TiTe <sub>3</sub> O <sub>8</sub> Ceramic Composites. Journal of the American Ceramic Society, 2011, 94, 812-816.	3.8	16
143	Porous Ni/8YSZ anode of SOFC fabricated by the plasma sprayed method. International Journal of Hydrogen Energy, 2012, 37, 13746-13754.	7.1	16
144	Effects of Nb2O5, TiO2, SiO2, and CaO additions on the loss characteristics of Mn-Zn Ferrite. Journal of Electroceramics, 2014, 33, 172-179.	2.0	16

#	Article	IF	CITATIONS
145	A Facile Chemical Synthesis of Cu <sub>2</sub> O Nanocubes Covered with Co <sub>3</sub> O <sub>4</sub> Nanohexagons for the Sensitive Detection of Glucose. Electroanalysis, 2016, 28, 1547-1552.	2.9	16
146	Effects of Sc2O3 and MgO additions on the dielectric properties of BaTiO3-based X8R materials. Journal of Alloys and Compounds, 2018, 768, 122-129.	5.5	16
147	Selective Electrochemical Sensing Platform Based on the Synergy between Carbon Black and Single-Crystalline Bismuth Sulfide for Rapid Analysis of Antipyretic Drugs. ACS Applied Bio Materials, 2021, 4, 7497-7508.	4.6	16
148	Densification, microstructure and microwave dielectric properties of ultra-low fire BaTe4O9–TiTe3O8 ceramic composites. Journal of the European Ceramic Society, 2010, 30, 1737-1741.	5.7	15
149	Microwave dielectric properties of multi-ions Ba(Zn,Ta)O3-based perovskite ceramics. Ceramics International, 2012, 38, 1127-1132.	4.8	15
150	Characteristics of LaCo0.4Ni0.6-xCuxO3-δ ceramics as a cathode material for intermediate-temperature solid oxide fuel cells. Journal of the European Ceramic Society, 2018, 38, 1654-1662.	5.7	15
151	Dry particle coating preparation of highly conductive LaMnO3@C composite for the oxygen reduction reaction and hydrogen peroxide sensing. Journal of the Taiwan Institute of Chemical Engineers, 2018, 93, 94-102.	5.3	15
152	Growth of 2D-layered double hydroxide nanorods heterojunction with 2D tungsten carbide nanocomposite: Improving the electrochemical sensing of norfloxacin. Journal of Industrial and Engineering Chemistry, 2022, 110, 434-446.	5.8	15
153	Phase stability of B2O3-added Ba2Ti9O20 ceramic: Processing effects. Journal of Materials Research, 2003, 18, 201-207.	2.6	14
154	Effect of SiO2 addition on the microstructure and microwave dielectric properties of ultra-low fire TiTe3O8 ceramics. Ceramics International, 2009, 35, 1813-1817.	4.8	14
155	A novel amperometric determination of flufenamic acid using CuMOF ribbons incorporated with activated carbon. New Journal of Chemistry, 2020, 44, 12586-12594.	2.8	14
156	Trace level electrochemical detection of mesalazine in human urine sample using poly (N-Vinyl)-2-Pyrrolidone capped Bi-EDTA complex sheets incorporated with ultrasonically exfoliated graphene oxide. Journal of the Taiwan Institute of Chemical Engineers, 2021, 122, 67-77.	5.3	14
	Green Synthesis of Magnetic Ferrites (Fe <sub>3</sub> O <sub>4</sub> ,) Tj ETQq1 1 0.784314 rgBT /Overlock 10	) Tf 50 26	7 Td (CoFe
157	Extract for Cancer Hyperthermia Activities. IEEE Transactions on Magnetics, 2022, 58, 1-7.	2.1	14
158	Effects of B <sub>2</sub> O <sub>3</sub> on the Phase Stability of Ba <sub>2</sub> Ti <sub>9</sub> O <sub>20</sub> Microwave Ceramic. Journal of the American Ceramic Society, 2002, 85, 1619-1621.	3.8	13
159	Effects of microstructure and CaO addition on the magnetic and mechanical properties of NiCuZn ferrites. Journal of Magnetism and Magnetic Materials, 2015, 394, 470-476.	2.3	13
160	A glassy carbon electrode modified with graphene oxide decorated silver phosphate nanodentrites for amperometric determination of dissolved hydrazine. Mikrochimica Acta, 2017, 184, 2569-2577.	5.0	13
161	Processing of Ce0.8Gd0.2O2-δ barrier layers for solid oxide cells: The effect of preparation method and thickness on the interdiffusion and electrochemical performance. Journal of the European Ceramic Society, 2020, 40, 5626-5633.	5.7	13
162	Highly selective electrochemical detection of diphenylamine in apple samples using rod shaped CuCo2O4 derived from bimetallic organic frameworks. Microchemical Journal, 2021, 165, 106146.	4.5	13

#	Article	IF	CITATIONS
163	Wettability of electrode metals on barium titanate substrate. Journal of Materials Science, 2001, 36, 825-829.	3.7	12
164	Preparation and Characterization of Polyimide/Zirconia Composite Films. Journal of Electronic Materials, 2008, 37, 925-929.	2.2	12
165	Densification, microstructural evolution, and dielectric properties of CaTiO3–LaGaO3 microwave ceramics. Journal of Physics and Chemistry of Solids, 2011, 72, 1011-1014.	4.0	12
166	Characteristics of Bilayer Molybdenum Films Deposited Using RF Sputtering for Back Contact of Thin Film Solar Cells. Advances in Materials Science and Engineering, 2014, 2014, 1-6.	1.8	12
167	Effect of Ta2O5 and Nb2O5 Dopants on the Stable Dielectric Properties of BaTiO3–(Bi0.5Na0.5)TiO3-Based Materials. Applied Sciences (Switzerland), 2015, 5, 1221-1234.	2.5	12
168	Effects of La2O3, Nd2O3, NiO and CoO additions on the characteristics of SiO2–Al2O3–Y2O3–ZnO glass seals for intermediate temperature solid oxide fuel cells. International Journal of Hydrogen Energy, 2015, 40, 3338-3347.	7.1	12
169	Simple preparation of birnessite-type MnO2 nanoflakes with multi-walled carbon nanotubes for the sensitive detection of hydrogen peroxide. Ionics, 2017, 23, 3219-3226.	2.4	12
170	A fascinating multifunctional bis(2-(4,5-diphenyl-1H-imidazol-2-yl)phenoxy)nickel complex: An excellent electrode material for supercapacitor and uric acid sensor. Materials Research Bulletin, 2019, 118, 110482.	5.2	12
171	Simple and Highly Selective Electrochemical Sensor Constructed Using Silver Molybdate Nano-Wire Modified Electrodes for the Determination of Oxidative Stress Biomarker in Blood Serum and Lens Cleaning Solution. Journal of the Electrochemical Society, 2020, 167, 147501.	2.9	12
172	High-performance anode-supported solid oxide fuel cells with co-fired Sm0.2Ce0.8O2-Î/La0.8Sr0.2Ga0.8Mg0.2O3â~Î/Sm0.2Ce0.8O2-Î′ sandwiched electrolyte. International Journal of Hydrogen Energy, 2022, 47, 5429-5438.	7.1	12
173	Electrochemical properties of myoglobin deposited on multi-walled carbon nanotube/ciprofloxacin film. Colloids and Surfaces B: Biointerfaces, 2011, 82, 526-531.	5.0	11
174	Improving biodegradation behavior of calcium sulfate bone graft tablet by using water vapor treatment. Materials Science and Engineering C, 2013, 33, 121-126.	7.3	11
175	High-performance NdSrCo2O5+Î′–Ce0.8Gd0.2O2-Î′ composite cathodes for electrolyte-supported microtubular solid oxide fuel cells. International Journal of Hydrogen Energy, 2021, 46, 31778-31787.	7.1	11
176	Exsolution of Ni nanoparticles on the surface of cerium and nickel co-doped lanthanum strontium titanate as a new anodic layer for DIR-SOFC. Anti-coking potential and H2S poisoning resistance of the prepared material. International Journal of Hydrogen Energy, 2020, 45, 29186-29200.	7.1	11
177	A study on Ti-doped Fe3O4 anode for Li ion battery using machine learning, electrochemical and distribution function of relaxation times (DFRTs) analyses. Scientific Reports, 2022, 12, 4851.	3.3	11
178	Synthesis of transition metal titanium oxide (MTiOx, MÂ=ÂMn, Fe, Cu) and its application in furazolidone electrochemical sensor. Journal of Industrial and Engineering Chemistry, 2022, 111, 356-368.	5.8	11
179	CALCIUM AND STRONTIUM DOPED ZnO FILMS FOR LOVE WAVE SENSOR APPLICATIONS. Integrated Ferroelectrics, 2005, 72, 13-22.	0.7	10
180	Synthesis and Characterization of Ce <sup>3+</sup> :YAG Phosphors by Heterogeneous Precipitation Using Different Alumina Sources. International Journal of Applied Ceramic Technology, 2009, 6, 470-478.	2.1	10

#	Article	IF	CITATIONS
181	Effects of silver oxalate additions on the physical characteristics of low-temperature-curing MOD silver paste for thick-film applications. Microelectronic Engineering, 2009, 86, 2316-2319.	2.4	10
182	Ultra‣owâ€Fire Te <sub>2</sub> (Mo <sub>1â^'<i>x</i></sub> W <i><sub>x</sub></i> )O <sub>7</sub> Ceramics: Microstructure and Microwave Dielectric Properties. Journal of the American Ceramic Society, 2010, 93, 4071-4074.	3.8	10
183	Solid oxide fuel cells with Sm0.2Ce0.8O2â~δ electrolyte film deposited by novel aerosol deposition method. Journal of Power Sources, 2011, 196, 5064-5069.	7.8	10
184	Effects of Nb5+, Mo6+, and W6+ dopants on the germanate-based apatites as electrolyte for use in solid oxide fuel cells. International Journal of Hydrogen Energy, 2013, 38, 12015-12023.	7.1	10
185	Enhanced coercivity of HCP Co–Pt alloy thin films on a glass substrate at room temperature for patterned media. Journal of Magnetism and Magnetic Materials, 2015, 391, 12-16.	2.3	10
186	Characteristics of copper-doped SrFe0.75Mo0.25O3â^δ ceramic as a cathode material for solid oxide fuel cells. Solid State Ionics, 2016, 296, 120-126.	2.7	10
187	Resistive switching characteristics of a spinel ZnAl2O4 thin film prepared by radio frequency sputtering. Ceramics International, 2016, 42, 17673-17679.	4.8	10
188	Solid oxide fuel cells with apatite-type lanthanum silicate-based electrolyte films deposited by radio frequency magnetron sputtering. Journal of Power Sources, 2018, 381, 101-106.	7.8	10
189	Effects of MnO addition on the stable dielectric properties of BaTiO3- (Bi0.5Na0.5)TiO3-Ta2O5 ceramics. Ceramics International, 2018, 44, 17038-17043.	4.8	10
190	Design and characterization of apatite La9.8Si5.7Mg0.3O26±δ-based micro-tubular solid oxide fuel cells. Journal of Power Sources, 2020, 460, 228072.	7.8	10
191	High-Performance Electrochemical Sensor Based on Yttrium Sulfide Nanoparticles Decorated Carbon Nitride Heterostructure for Highly Sensitive Detection of Antimicrobial Drug in Biological Samples. Journal of the Electrochemical Society, 2021, 168, 077516.	2.9	10
192	Hydrothermal-Dependent Synthesis of Exfoliated Nickel Cobaltite Layers for Simultaneous Determination of IARC Group 2B, 3B Carcinogens. ACS Applied Nano Materials, 2021, 4, 12788-12797.	5.0	10
193	Pt Nanoparticle-Decorated Se Rods for Electrochemical Detection of 17β-Estradiol and Methanol Oxidation. ACS Applied Nano Materials, 2022, 5, 1944-1957.	5.0	10
194	Physical and structural characteristics of sol–gel derived CaO–B2O3–SiO2 glass-ceramics and their dielectric properties in the 5G millimeter-wave bands. Ceramics International, 2022, 48, 9030-9037.	4.8	10
195	Amperometric detection of antibiotic drug ciprofloxacin using cobalt-iron Prussian blue analogs capped on carbon nitride. Mikrochimica Acta, 2022, 189, 31.	5.0	10
196	Biomass-derived porous activated carbon from <i>anacardium occidentale</i> shell as electrode material for supercapacitors. New Journal of Chemistry, 2022, 46, 8863-8873.	2.8	10
197	Hierarchically Ordered Tungsten Antimonate Nanoflowers Anchored on Carbon Nanofibers for Electrochemical Detection of a Food Additive. ACS Applied Nano Materials, 2022, 5, 10331-10340.	5.0	10
198	Effects of CaTiO <sub>3</sub> and SrTiO <sub>3</sub> Additions on the Microstructure and Microwave Dielectric Properties of Ultra‣owâ€Fire TeO <sub>2</sub> Ceramics. Journal of the American Ceramic Society, 2010, 93, 3272-3277.	3.8	9

#	Article	IF	CITATIONS
199	Effects of Additives on the Densification and Microwave Dielectric Properties of Binary CaO–B <sub>2</sub> O <sub>3</sub> –SiO <sub>2</sub> Glass. Japanese Journal of Applied Physics, 2010, 49, 021101.	1.5	9
200	Fabrication of L11 Co-Pt-Cu perpendicular anisotropic films with enhanced coercivity on glass substrate. Journal of Applied Physics, 2012, 111, 07A706.	2.5	9
201	Microstructures and Dielectric Properties of MgTiO3Thick Film Prepared Using Aerosol Deposition Method. Ferroelectrics, 2012, 435, 137-147.	0.6	9
202	Microwave dielectric properties of (Ba1â^'Sr )(Mg0.5W0.5)O3 ceramics. Ceramics International, 2015, 41, 8931-8935.	4.8	9
203	Effects of addition of Sc2O3 on microstructure and dielectric properties of BaTiO3-based X8R MLCCs. Journal of Physics and Chemistry of Solids, 2019, 127, 194-201.	4.0	9
204	Fabrication of polystyrene/carbon nanocomposites with superior mechanical properties. Polymer Engineering and Science, 2020, 60, 2046-2056.	3.1	9
205	Dielectric Behavior and Second Phases in X7Râ€Formulated BaTiO <sub>3</sub> Sintered in Lowâ€Oxygen Partial Pressures. Journal of the American Ceramic Society, 2007, 90, 2926-2934.	3.8	8
206	Synthetic antibacterial agent assisted synthesis of gold nanoparticles: Characterization and application studies. Journal of Physics and Chemistry of Solids, 2010, 71, 1484-1490.	4.0	8
207	Perpendicular magnetic anisotropic Pr-Fe-B thin films on glass substrates. Journal of Applied Physics, 2014, 115, .	2.5	8
208	Solid oxide fuel cells with (La,Sr)(Ga,Mg)O 3-δelectrolyte film deposited by radio-frequency magnetron sputtering. Journal of Power Sources, 2015, 281, 258-264.	7.8	8
209	Evaluation of Osseointegration in Titanium and Zirconia-Based Dental Implants with Surface Modification in a Miniature Pig Model. Journal of Medical and Biological Engineering, 2017, 37, 313-320.	1.8	8
210	Synthesis of Carbon Dots on Fe <sub>3</sub> O <sub>4</sub> Nanoparticles as Recyclable Visible-Light Photocatalysts. IEEE Transactions on Magnetics, 2017, 53, 1-4.	2.1	8
211	Characteristics of La <sub>0.8</sub> Sr <sub>0.2</sub> Ga <sub>0.8</sub> Mg <sub>0.2</sub> O <sub>3−δ</sub> -support micro-tubular solid oxide fuel cells with bi-layer and tri-layer electrolytes. Journal of the Ceramic Society of Japan, 2017, 125, 236-241.	orted 1.1	8
212	Fabrication of Magnetic Fe <sub>3</sub> O <sub>4</sub> Nanoparticles with Unidirectional Extension Pattern by a Facile and Eco-Friendly Microwave-Assisted Solvothermal Method. Journal of Nanoscience and Nanotechnology, 2019, 19, 7645-7653.	0.9	8
213	Electrochemical determination of Hg2+ in sakura shrimp and drinking water using f-CNF/TeO2 composite. Journal of Materials Science: Materials in Electronics, 2020, 31, 12973-12982.	2.2	8
214	Investigations of the effective parameters on the synthesis of monodispersed magnetic Fe3O4 by solvothermal method for biomedical applications. AIP Advances, 2020, 10, .	1.3	8
215	Interface study of diamond films grown on (100) silicon. Thin Solid Films, 2006, 498, 224-229.	1.8	7
216	Microstructures and microwave dielectric properties of Li2O–Nb2O5–ZrO2 ceramics. Ceramics International, 2007, 33, 1389-1393.	4.8	7

#	Article	IF	CITATIONS
217	Effects of Nd/Sm ratio and glass addition on the microwave dielectric properties of Ba4.5(Sm(0.8â^'x)NdxBi0.2)9Ti18O54 ceramics. Journal of Alloys and Compounds, 2009, 468, 522-527.	5.5	7
218	Densification, microstructural evolution and microwave dielectric properties of fluxed sintered 12R-Ba(Ti0.5Mn0.5)O3 ceramics. Ceramics International, 2011, 37, 1327-1331.	4.8	7
219	Effects of CaTiO3 addition on the densification and microwave dielectric properties of BiSbO4 ceramics. Ceramics International, 2013, 39, 2857-2861.	4.8	7
220	Properties and Performance of La <sub>2</sub> NiO <sub>4+δ</sub> -LaNiO <sub>3</sub> Composite Cathodes for Intermediate-Temperature Solid Oxide Fuel Cells. Ferroelectrics, 2013, 457, 105-110.	0.6	7
221	Effects of cathode materials on the characteristics of electrolyte supported micro-tubular solid oxide fuel cells. Journal of Power Sources, 2014, 253, 35-40.	7.8	7
222	Effects of Thickness Ratio of Co to Pt Layer on Magnetic Properties and Microstructure of [Co/Pt] <sub><italic>n</italic></sub> Multilayer Films. IEEE Transactions on Magnetics, 2015, 51, 1-4.	2.1	7
223	Highly Sensitive Hydrazine Sensor Based on Co(OH) <sub>2</sub> Nanoflakes Electrochemically Deposited on MWCNTs. Electroanalysis, 2017, 29, 1088-1094.	2.9	7
224	Honeycomb oxygen-generator with doped bismuth-oxide-based electrolyte and Ag electrode. Journal of Electroceramics, 2020, 44, 104-111.	2.0	7
225	CoFe <sub>2</sub> O <sub>4</sub> supported g-C <sub>3</sub> N <sub>4</sub> nanocomposite for the sensitive electrochemical detection of dopamine. New Journal of Chemistry, 2021, 45, 18131-18138.	2.8	7
226	Physical and sealing properties of BaO–Al2O3–SiO2–CaO–V2O5 glasses for solid oxide fuel cell applications. International Journal of Hydrogen Energy, 2022, 47, 10044-10055.	7.1	7
227	Effects of Bi2Mo2O9 addition on the sintering characteristics and microwave dielectric properties of BiSbO4 ceramics. Journal of the European Ceramic Society, 2011, 31, 2975-2980.	5.7	6
228	Solid oxide fuel cells with YSZ-BNO Bi-layer electrolyte film deposited by magnetron sputtering. Ceramics International, 2011, 37, 2095-2100.	4.8	6
229	SrCo1â^'xSbxO3â^´Î´ cathode materials prepared by Pechini method for solid oxide fuel cell applications. Ceramics International, 2012, 38, 5941-5947.	4.8	6
230	Sr1â^'xPrxCo0.95Sn0.05O3â^'δ ceramic as a cathode material for intermediate-temperature solid oxide fuel cells. International Journal of Hydrogen Energy, 2012, 37, 12548-12556.	7.1	6
231	Electrical Properties and Microstructural Analysis of Aliovalent-Ion (Y3+, Nb5+)–Doped Bismuth-Based Solid-Oxide Electrolyte. Ferroelectrics, 2013, 455, 123-128.	0.6	6
232	Fast Oxidation of Porous Cu Induced by Nano-Twinning. Inorganic Chemistry, 2018, 57, 2908-2916.	4.0	6
233	The Sputtering of Heusler Alloy Catalyst onto the Porous Anode of the Intermediate Temperature Solid Oxide Fuel Cells for Ammonia Disassociation. ECS Transactions, 2019, 91, 361-365.	0.5	6
234	An effective morphology controlled hydrothermal synthesis of Bi2WO6 and its application in riboflavin electrochemical sensor. Colloids and Surfaces A: Physicochemical and Engineering Aspects, 2022, 648, 129183.	4.7	6

#	Article	IF	CITATIONS
235	Stacking Faults and Stacking Fault Energy of Hexagonal Barium Titanate. Journal of the American Ceramic Society, 2006, 89, 3778-3787.	3.8	5
236	Microstructure and Electrical Resistivity of Low-Temperature-Cured Silver Films Prepared Using Silver Oxide and Silver Stearate Pastes. Japanese Journal of Applied Physics, 2009, 48, 016501.	1.5	5
237	Conducting filaments in Pt/ZrCuOy/Pt resistive switching memory cells. Materials Chemistry and Physics, 2015, 168, 95-100.	4.0	5
238	Facile Synthesis of Graphene/Cobalt Oxide Nanohexagons for the Selective Detection of Dopamine. Electroanalysis, 2017, 29, 923-928.	2.9	5
239	Room temperature deposition of perpendicular magnetic anisotropic Co3Pt thin films on glass substrate. Journal of Magnetism and Magnetic Materials, 2017, 425, 57-62.	2.3	5
240	Solid oxide fuel cells incorporating doped lanthanum gallate films deposited by radio-frequency magnetron sputtering at various Ar/O2 ratios and annealing conditions. Surface and Coatings Technology, 2018, 344, 507-513.	4.8	5
241	Characteristics of Honeycomb-Type Oxygen Generator with Electrolyte Based on Doped Bismuth Oxide. Journal of Electronic Materials, 2018, 47, 3639-3646.	2.2	5
242	Effects of Na+, K+ and B3+ Substitutions on the Electrical Properties of La10Si6O27 Ceramics. Journal of Electronic Materials, 2019, 48, 6287-6297.	2.2	5
243	Simple preparation of gold nanoparticle-decorated copper cross-linked pectin for the sensitive determination of hydrogen peroxide. Ionics, 2019, 25, 309-317.	2.4	5
244	The characteristics of inorganic electroluminescent devices with an amorphous diamond film as cathode material. Thin Solid Films, 2009, 517, 1821-1824.	1.8	4
245	Thermal Conductivity of Diamond-Containing Grease. Journal of Electronic Packaging, Transactions of the ASME, 2010, 132, .	1.8	4
246	Fabrication of <italic>L</italic> 1 <sub>1</sub> Phase CoPt Film on Glass Substrate With [Co/Pt] Multilayer Structure. IEEE Transactions on Magnetics, 2014, 50, 1-4.	2.1	4
247	The effects of boron dopant on the thermal stability, semiconductor characteristic and wear resistance of diamond films. Materials Research Innovations, 2017, 21, 358-366.	2.3	4
248	Oxide composite prepared from intermetallic and amorphous Zr67Fe30M3- (M=Au, Pt) alloys and their catalytic activity for CO oxidation. Journal of Physics and Chemistry of Solids, 2017, 100, 49-56.	4.0	4
249	Distribution of relaxation times as a method of separation and identification of complex processes measured by impedance spectroscopy. , 2017, , .		4
250	Characteristics of La0.8Sr0.2Ga0.8Mg0.2O3-δ-supported micro-tubular solid oxide fuel cells with LaCo0.4Ni0.6-xCuxO3-δ cathodes. International Journal of Hydrogen Energy, 2018, 43, 5703-5713.	7.1	4
251	Hydrogen production of nickel–scandia-stabilized zirconia and copper/nickel–scandia-stabilized zirconia catalysts through steam methane reforming for solid oxide fuel cell operation. Clean Technologies and Environmental Policy, 2018, 20, 2067-2074.	4.1	4
252	Methyl Orange Adsorption onto Magnetic Fe <sub>3</sub> O <sub>4</sub> /Carbon (AC, GO, PGO) Nanocomposites. Journal of Nanoscience and Nanotechnology, 2021, 21, 5756-5764.	0.9	4

#	Article	IF	CITATIONS
253	Synergetic effect of the ultrasonic-assisted hydrothermal process on the photocatalytic performance of MoS2 and WS2 nanoparticles. Journal of Materials Science: Materials in Electronics, 2022, 33, 8858-8867.	2.2	4
254	Integration of iron–manganese layered double hydroxide/tungsten carbide composite: An electrochemical tool for diphenylamine H•+ analysis in environmental samples. Environmental Research, 2022, 212, 113291.	7.5	4
255	Synthesis of Gold Nanorods/Nanobelts and Their Potent Electrocatalytic Properties toward Ethanol Oxidation. Chemistry Letters, 2010, 39, 74-75.	1.3	3
256	Resistive Switching Characteristics of 10-nm-Thick Amorphous HoScO x Films Doped with Nb and Zn. Journal of Electronic Materials, 2017, 46, 1488-1496.	2.2	3
257	Onset of hard magnetic MnGa thin film on glass substrate. Journal of Magnetism and Magnetic Materials, 2021, 524, 167668.	2.3	3
258	Effects of La0.8Sr0.2MnO3 and Ag electrodes on bismuth-oxide-based low-temperature solid electrolyte oxygen generators. Ceramics International, 2022, 48, 1132-1141.	4.8	3
259	Silver-capped selenium explored as an electro-catalyst for simultaneous detection of nitro-aromatic drugs in different aqueous samples. Journal of Industrial and Engineering Chemistry, 2022, 108, 243-253.	5.8	3
260	A Biocompatible Design of Kappa-Carrageenan/Functionalized-Boron Nitride Nanocomposite: The Disposable Electrode of Mercury Detection. Journal of the Electrochemical Society, 0, , .	2.9	3
261	Aerosol Plasma Deposition Method for Preparation of Lead Zirconate Titanate Thick Films. Japanese Journal of Applied Physics, 2005, 44, 3240-3241.	1.5	2
262	A planar chip antenna for 2.4/5.2GHz ISM band applications. , 2005, , .		2
263	High-Frequency Electrical Properties of Silver Thick Films Measured by Dielectric Resonator Method. Japanese Journal of Applied Physics, 2008, 47, 7289-7294.	1.5	2
264	Compact chip antenna applications in GPS by LTCC processing. Microwave and Optical Technology Letters, 2009, 51, 1017-1019.	1.4	2
265	Characteristics of silver powders synthesized from silver 2-ethylhexanoate and Di-n-octylamine. Journal of Electroceramics, 2013, 31, 109-116.	2.0	2
266	The Structure-Property-Processing Relationship for Sintered Yttria-Stabilized Zirconia (YSZ)/Alumina Bioceramics. Biomedical Engineering - Applications, Basis and Communications, 2013, 25, 1350005.	0.6	2
267	Resistance switching behaviors of amorphous (ZrTiNi)Ox films for nonvolatile memory devices. Journal of Vacuum Science and Technology A: Vacuum, Surfaces and Films, 2014, 32, 061505.	2.1	2
268	Microwave dielectric properties of ZrO2 and SnO2 doped Ca5Nb4TiO17 ceramics. Journal of Alloys and Compounds, 2016, 679, 254-259.	5.5	2
269	Dielectric properties and microstructures of non-reducible high-temperature stable dielectrics based on 0.9474BaTiO 3 -0.0526Ba 2 LiTa 5 O 15. Ceramics International, 2017, 43, S79-S84.	4.8	2
270	The influence of synthesis method on the microstructure and catalytic performance of Y0.07Sr0.93Ti0.8Fe0.2O3-l´ in synthetic biogas operated solid oxide fuel cells. Materials Research Bulletin, 2018, 100, 49-55.	5.2	2

#	Article	IF	CITATIONS
271	Effects of Na+, K+ and B3+ Substitutions on the Electrical Properties of La10Si6O27 Ceramics. ECS Transactions, 2019, 91, 1223-1228.	0.5	2
272	Sub-10â€ <sup>-</sup> nm multicomponent oxide with forming-free resistive switching characteristics. Thin Solid Films, 2019, 688, 137450.	1.8	2
273	Characterization of new catalysts prepared by in-situ activation of Ce50Ni50-xAux intermetallic compounds for CO oxidation. Intermetallics, 2020, 120, 106748.	3.9	2
274	Enhanced Perpendicular Magnetic Anisotropy of Co-Rich Type Co–Pt Film by Inserting Pt Underlayer. IEEE Transactions on Magnetics, 2015, 51, 1-4.	2.1	1
275	Effects of Li <sup>+</sup> and Mg <sup>2+</sup> Dopants on the Magnetic Properties of Ni–Zn Ferrites. IEEE Transactions on Magnetics, 2015, 51, 1-7.	2.1	1
276	Effects of La content on the densification, microstructure, and conductivity of doped La <sub>10â^'<i>x</i></sub> Ge <sub>6</sub> O <sub>26±Î′</sub> electrolytes. International Journal of Applied Ceramic Technology, 2017, 14, 84-93.	2.1	1
277	DC bias characteristics of BaTi0.65Zr0.35O3 with additives (Gd2O3, SiO2, MgO) for multilayer ceramic capacitors. Ceramics International, 2020, 46, 28227-28236.	4.8	1
278	Low-Temperature Planar Oxygen Generator with (Bi1.50Y0.50)0.98Zr0.04O3+Î′/Bi1.71Nb0.25Ba0.04O3+Î′ Dual-Layer Electrolyte Membrane. Journal of Electronic Materials, 2021, 50, 4155.	2.2	1
279	Kinetic Analysis and Modeling of Poly(Vinyl Butyral)/Glass Ceramic/Metal Thermal Oxidative Degradation Using Thermogravimetric Analysis and Neural Networks. Journal of Chemical Engineering of Japan, 2004, 37, 204-209.	0.6	1
280	Effect of a Rubidium Chloride Carrier Confinement Layer on the Characteristics of CsPbBr3 Perovskite Light-Emitting Diodes. Nanoscale Research Letters, 2022, 17, 2.	5.7	1
281	Promotional effects of Pt–CeO2 fabricated by hydrothermal leaching of Al78Ce22-xPtx (x = 0, 0.1) intermetallic compound for efficient catalytic CO oxidation. Journal of Solid State Chemistry, 2022, 309, 122984.	2.9	1
282	Volume effects on microstructures and magnetic properties of MnGa thin films during order-disorder transformation. Vacuum, 2022, , 111068.	3.5	1
283	Migration of Half Partial Dislocations in the Planar Fault Plane of Hexagonal Barium Titanate. Journal of the American Ceramic Society, 2007, 90, 230-237.	3.8	0
284	A compact cascade quadruplet bandpass filter with low temperature cofired ceramic technology. Microwave and Optical Technology Letters, 2008, 50, 3218-3220.	1.4	0
285	Ba2Ti9O20Thick Films Deposited by Novel Aerosol Deposition Method. Japanese Journal of Applied Physics, 2009, 48, 041404.	1.5	0
286	Mixing PSO and Tabu search technique and its application to estimation of carrier frequency offsets for uplink OFDMA system. , 2014, , .		0
287	Effects of Reaction Conditions on the Properties of Spherical Silver Powders Synthesized by Reduction of an Organometallic Compound. Journal of Electronic Materials, 2014, 43, 3397-3403.	2.2	Ο
288	Gallium-doped lanthanum germanates as electrolyte material of solid oxide fuel cells. Journal of the Ceramic Society of Japan, 2015, 123, 222-228.	1.1	0

#	Article	IF	CITATIONS
289	Effects of WO3 and Ta2O5 Dopants on the Structure, Microstructure, and Microwave Dielectric Properties of Ca5Nb4TiO17 Ceramics. Journal of Electronic Materials, 2016, 45, 3030-3039.	2.2	Ο
290	Microwave Dielectric Properties of Ca4(La4Pr2)(SiO4)4(PO4)2O2 Ceramics Doped with Isovalent and Aliovalent Ions. Journal of Electronic Materials, 2019, 48, 6421-6430.	2.2	0
291	Effects of exit-stream mixtures of the steam reforming on the intermediate-temperature solid oxide fuel cells with nickel-based anodes. Journal of Solid State Electrochemistry, 2020, 24, 1305-1312.	2.5	0
292	Dielectric Properties and DC Bias Characteristics of BaTi1-mZrmO3-x mol.% MgO-4.5 mol.% Gd2O3-2 mol.% SiO2 Ceramics. Journal of Electronic Materials, 2021, 50, 5946-5954.	2.2	0
293	Effects of Ca2+, Mg2+, Na+, and K+ substitutions on the microstructure and electrical properties of GdCoO3 ceramics. Journal of Electroceramics, 2020, 45, 75-83.	2.0	0